scientific reports

Check for updates

OPEN

PET imaging of differentiated thyroid cancer with thyrotropin-alfa

Grayson R. Gimblet[1], Pratheek Reddy[1], Michelle M. Holland[2], Hailey A. Houson[1], Jason Whitt[2], John A. Copland[3], Saad S. Kenderian[4], Renata Jaskula-Sztul[2]✉ & Suzanne E. Lapi[1]✉

Thyrotropin-alfa is an FDA approved recombinant human TSH agonist. This study represents a preclinical evaluation of thyrotropin-alfa as a thyroid-stimulating hormone receptor (TSHR)-targeted PET radiopharmaceutical, [^{89}Zr]Zr-thyrotropin-alfa. [^{89}Zr]Zr-thyrotropin-alfa was synthesized by conjugating p-SCN-Bn-deferoxamine (DFO) to thyrotropin-alfa in a molar ratio of 3:1 (DFO:thyrotropin-alfa) and radiolabeling with ^{89}Zr ($t_{1/2}$ = 78.4 h, β^+ = 22.7%) at a molar activity of 25.9 MBq/nmol. [^{89}Zr]Zr-thyrotropin-alfa uptake was assessed in THJ529T and FTC133 cells stably transduced with the TSHR and compared to their low-expressing wild-type. Studies included a combination of *in vitro* cell uptake, *in vivo* PET imaging, and *ex vivo* biodistribution on Days 1–3 post-injection in male and female mice. *In vitro* uptake was significantly higher ($P < 0.0001$) in TSHR + THJ529T (6.6 ± 1.3% bound/mg) and FTC133 (3.5 ± 0.5% bound/mg) cells over low-expressing wild-type counterparts (2.9 ± 1.3% bound/mg and 2.0 ± 0.4% bound/mg, respectively). Blocking uptake with excess DFO-thyrotropin-alfa showed specificity for TSHR ($P < 0.0001$). *In vivo* PET imaging showed the highest uptake in TSHR + xenografts on Day 1 post-injection. *Ex vivo* biodistribution demonstrated significantly higher uptake in the TSHR + female FTC133 xenograft model ($P < 0.0001$) and TSHR + male FTC133 xenograft model ($P < 0.0001$) compared to TSHR- xenografts. Uptake of [^{89}Zr]Zr-thyrotropin-alfa supports continued preclinical optimization and potential studies in clinical trials.

Keywords Thyroid, DTC, PET, Thyrotropin-alfa, TSHR

Thyroid cancer is the most common endocrine cancer in the United States, accounting for over 40,000 annual cases, with a three-fold higher incidence in women[1]. Of the major histological types of thyroid cancer[2], differentiated thyroid carcinomas (DTCs) make up 95% of diagnoses[3].

Most patients with DTC will undergo successful surgical resection of their disease, with adjuvant radioiodine therapy given for patients with intermediate or high-risk disease features[4–6]. However, it is known that a subset of patients with DTC, up to 20%, will become radioiodine refractory, with metastatic disease presenting as a substantial risk factor[7,8]. Consequently, patients with radioiodine refractory disease have 5-year and 10-year survival rates of 60% and 10%, respectively[7,9].

A new molecular target, such as the thyroid-stimulating hormone receptor (TSHR), has the potential to offer an alternative theranostic approach for patients with radioiodine refractory disease. The TSHR is a class A G-protein-coupled-receptor (GPCR), which is a target for endogenous thyroid-stimulating hormone (TSH) to mediate the release of thyroid hormone and thyroid gland function[10]. Recent work has focused on the development of diagnostic single photon emission computed tomography (SPECT) and positron emission tomography (PET) radiopharmaceuticals targeting the TSHR using recombinant human TSH analogue TR1402[11–13]. Such an imaging approach is not only clinically useful for diagnosis but can also help identify candidates for TSHR-targeted therapies with small molecule antagonists[14] or CAR-T cells[15].

Thyrotropin-alfa is a recombinant form of human TSH initially approved by the US FDA in 1998 as an adjuvant diagnostic tool for serum thyroglobulin testing[16]. In 2007, thyrotropin-alfa was approved by the FDA as an adjunct treatment for radioiodine ablation of thyroid tissue remnants[17,18]. The translation of thyrotropin-

[1]Department of Radiology, University of Alabama at Birmingham, Birmingham, AL, USA. [2]Department of Surgery, University of Alabama at Birmingham, Birmingham, AL, USA. [3]Department of Cancer Biology, Mayo Clinic Jacksonville, Jacksonville, FL, USA. [4]Division of Hematology, Mayo Clinic Rochester, Rochester, MN, USA. ✉email: ; lapi@uab.edu

alfa into a diagnostic radiopharmaceutical has the potential for high clinical impact in patients with radioiodine refractory disease.

Preclinical SPECT imaging in a mouse model with radioiodinated thyrotropin-alfa has been previously reported[19]. Using ^{123}I ($t_{1/2}$ = 13.2 h), mice were injected with 10 µg [^{123}I]I-thyrotropin-alfa and imaged up to three hours post-injection[19]. Expanding on this work, this study explores the preclinical potential of thyrotropin-alfa radiolabeled with ^{89}Zr ($t_{1/2}$ = 78.4 h), a PET radioisotope offering higher sensitivity and temporal resolution compared to SPECT imaging[20]. In this study, the suitability of [^{89}Zr]Zr-thyrotropin-alfa as a radiopharmaceutical is assessed through a combination of *in vitro* cell uptake, *in vivo* PET imaging, and *ex vivo* biodistribution.

Materials and methods

For this prospective preclinical animal study, all materials were purchased from Thermo Fisher Scientific (Waltham, MA, USA) unless otherwise noted. All animal procedures were approved by the University of Alabama at Birmingham (UAB) IACUC through animal protocol number IACUC-22598 were performed in accordance with relevant guidelines and regulations and are reported in accordance with ARRIVE guidelines.

Zirconium-89 (^{89}Zr) production

Zirconium-89 ($t_{1/2}$=78.4 h, β^+ = 22.7%) was produced as the oxalate salt by the UAB Cyclotron Facility on an ACSI TR-24 cyclotron, as previously described[21], and was used within one week of production.

Thyrotropin-alfa radiolabeling

Thyrotropin-alfa (Thyrogen) (NDC-58468-0030–2) (Sanofi, Bridgewater, NJ) is a recombinant human TSH analogue (23.7 kDa) that was purchased commercially and received as a lyophilized powder. Upon receipt, thyrotropin-alfa was reconstituted in water, alliquoted, and stored at −80°C.

Acyclic chelator p-SCN-Bn-deferoxamine (DFO) (Macrocyclics, Plano, TX) was conjugated to thyrotropin-alfa in a molar ratio of 3:1 (DFO:thyrotropin-alfa) in pH 9 0.1 M sodium carbonate for two hours at 37 °C, as previously described[22]. The product was buffer exchanged into 1 M HEPES using a Zeba Micro Spin Desalting Column 7k MWCO, 75 µL. The conjugated product DFO-thyrotropin-alfa was radiolabeled with pH 7 neutralized ^{89}Zr ($t_{1/2}$ = 78.4 h, β^+ = 22.7%) for one hour at 37 °C in 1 M HEPES to produce [^{89}Zr]Zr-thyrotropin-alfa with a molar activity of 25.9 MBq/nmol (25 µCi/µg).

Radiochemical purity was assessed with instant thin-layer chromatography silica gel (iTLC-SG) strips (Agilent Technologies, Santa Clara, CA) and size-exclusion high-performance liquid chromatography (Agilent Technologies 1260 Infinity HPLC) with a TSKgel UP-SW3000-LS column (Tosoh Bioscience, Philadelphia, PA). iTLC-SG strips were developed in a 50 mM DTPA (Acros Organics, Waltham, MA) mobile phase and read on an AR-2000 TLC scanner (Eckert and Ziegler, Hopkinton, MA). For HPLC, a 30 min isocratic gradient consisting of 50 mM sodium phosphate, monobasic, monohydrate with 150 mM sodium chloride and 0.1% Tween-20 at pH 7 was used. The stability of [^{89}Zr]Zr-thyrotropin-alfa was assessed over seven days by incubation with either mouse serum or 0.9% saline (Farris Laboratories, Fort Worth, TX) at 37 °C. The percent of intact radiotracer was determined by iTLC.

Cell culture

The human thyroid cancer cell lines THJ529T and FTC133 used in this study were provided by Drs. Saad Kenderian (Mayo Clinic Rochester, MN) and John Copland (Mayo Clinic Jacksonville, FL) as a low-expressing wild-type (TSHR-) and TSHR-positive (TSHR+) model, previously transduced with the full-length coding region of the human TSHR gene[12]. The absence of TSHR in commonly available DTC-derived cell lines is well-established[23–25], and contrasts sharply from the expression of TSHR in DTC patient lysates[12]. The absence of TSHR in cell culture has been attributed to the disruption of follicular architecture and loss of apical-basal polarity[26].

The THJ529T cell line was established by Marlow et al.[27] from a male patient with poorly differentiated thyroid carcinoma (PDTC) and was maintained in RPMI 1640 supplemented with 10% fetal bovine serum (FBS) and gentamicin. The FTC133 cell line was established by Goretzki et al.[27,28] from the lymph node metastasis of a male patient with follicular thyroid carcinoma (FTC) and was maintained in Dulbecco's Modified Eagle Medium (DMEM) supplemented with 10% FBS, gentamicin, and 10 µg/mL insulin (Millipore Sigma, Burlington, MA). Cells were grown in humidified incubators at 37 °C with 5% CO_2 in T175 flasks.

In vitro cell uptake

Cell uptake studies were performed with 250k TSHR + and wild-type THJ529T and FTC133 cells plated in 12-well plates 12–16 h prior to the study. Plated cells were incubated with 1 nM [^{89}Zr]Zr-thyrotropin-alfa in 400 µL of media for one hour at 37 °C in 5% CO_2, with 250 nM DFO-thyrotropin-alfa added in blocking wells. After incubation, cells were washed with 1 mL cold Dulbecco's Phosphate-Buffered Saline (DPBS) and lysed with 200 µL 0.2 M NaOH (Millipore Sigma, Burlington, MA, USA). The amount of radioactivity in lysed cells was quantified on a PerkinElmer 2480 automatic gamma counter (PerkinElmer, Waltham, MA, USA). A bicinchoninic acid (BCA) assay was used to normalize radioactive counts to protein concentration.

Binding affinity of [^{89}Zr]Zr-thyrotropin-alfa was determined by a radioactive binding assay with a one-site binding fit, accounting for nonspecific binding. Briefly, a 96-well breakable strip plate was coated at 3 µg/mL with 50 µL chimera recombinant human TSHR (rhTSHR) (Catalogue Number: 8950-TR) (R&D Systems, Minneapolis, MN, USA) dissolved in water. The plate was dried at 37 °C overnight and retrieved the next day. Blocking buffer (1% BSA in DPBS with 0.01% Tween) was added to each well and incubated for 1 h at RT. After incubation, the plate was dried and washed twice with a wash solution (DPBS + 0.5% Tween). A serial dilution was performed into 100 µL of blocking buffer with a starting concentration of 530 nM [^{89}Zr]Zr-thyrotropin-

alfa, for a final volume of 100 µL in each well. The plate was incubated for 2 h at RT with nutation. Following incubation, the plate was dried and washed x4 with the wash solution. The amount of radioactivity in individual wells was quantified on a PerkinElmer 2480 automatic gamma counter (PerkinElmer, Waltham, MA, USA).

Internalization of [^{89}Zr]Zr-thyrotropin-alfa was assessed as previously described[13]. Briefly, plated cells were incubated with 1 nM [^{89}Zr]Zr-thyrotropin-alfa for 5, 30, 60, or 120 min. Following incubation, cells were placed on ice and washed with 1 mL cold DPBS. Membrane-bound activity was stripped using 0.1 M pH 2 sodium citrate/citric acid buffer. Internalized activity was recovered by lysing cells with 200 µL 0.2 M NaOH (Millipore Sigma, Burlington, MA, USA). Radioactivity was quantified on a PerkinElmer 2480 automatic gamma counter (PerkinElmer, Waltham, MA, USA).

In vivo PET imaging

Male and female athymic nude mice (5 weeks old) were purchased from Charles River Laboratories (Wilmington, MA) and allowed to acclimate for at least 72 h prior to undergoing procedures. Subcutaneous xenografts were established in the left shoulder under 2% inhaled isoflurane anesthesia in oxygen at 2 L/min with 10^6 transduced TSHR + THJ529T and FTC133 cells suspended in 100 µL DPBS and 10^6 wild-type THJ529T and FTC133 cells suspended in 100 µL 1:1 PBS and Matrigel (Corning, Glendale, AZ). Xenografts were allowed to grow until reaching a size of 200–250 mm^3 within three weeks ($n = 4$ per group).

[^{89}Zr]Zr-thyrotropin-alfa was administered in the lateral tail vein under 2% inhaled isoflurane anesthesia in oxygen at 2 L/min. Mice were injected with 2 µg (1.6 ± 0.1 MBq) [^{89}Zr]Zr-thyrotropin-alfa in a volume of 100 µL isotonic saline. PET imaging was performed on three sequential days – 24 h, 48 h, and 72 h post-injection – on a GNEXT small animal PET/CT (Sophie, Springfield, VA). PET imaging data was acquired with a 25 min static scan followed by a 3 min CT (80 kVp). Dead time correction, decay correction, and attenuation correction based on the CT file were performed. VivoQuant 4.0 software (Invicro, Boston, MA) was used for imaging processing and SUV calculation.

Ex vivo biodistribution

Following Day 3 PET imaging, mice were euthanized by cervical dislocation under 5% isoflurane. Organs collected for *ex vivo* biodistribution studies were counted and weighed on a Hidex gamma counter (Lablogic, Clair-Mel City, FL).

Statistical analysis

Data from cell studies was compared with a one-way ANOVA ($\alpha = 0.05$) with a Bonferroni correction for multiple comparisons. Data obtained from PET imaging and *ex vivo* biodistribution were compared with multiple unpaired t-tests ($\alpha = 0.05$), with corrections for multiple comparisons made with the Bonferroni-Dunn method. Statistical analysis was performed in GraphPad Prism 9 (Dotmatics, Boston, MA). Statistical significance is indicated as $P < 0.05$ =*, $P < 0.01$ =**, $P < 0.001$=***, and $P < 0.0001$ =****.

Results

Radiolabeling and stability

High radiochemical purity (> 95%) was obtained by radiolabeling DFO-thyrotropin-alfa with ^{89}Zr as assessed by iTLC (Fig. **S1a**). The retention factor (R_f) for [^{89}Zr]Zr-thyrotropin-alfa was 0.0 and free [^{89}Zr]Zr-oxalate was 1.0 (Fig. **S1a**). On HPLC, there was > 95% purity (Fig. **S1b**) with no evidence of free ^{89}Zr or protein aggregates (Fig. **S1c**). Stability was assessed in 0.9% saline and mouse serum (Fig. **S1d**), with > 95% intact for up to seven days.

In Vitro Cell Uptake

Differentiated thyroid cancer cell lines THJ529T and FTC133 were used to assess *in vitro* cell uptake of [^{89}Zr]Zr-thyrotropin-alfa[12,27] (Fig. 1). Uptake in THJ529T + cells (6.6 ± 1.3% bound/mg) was significantly higher ($P < 0.0001$) than uptake in THJ529T- cells (2.9 ± 1.3% bound/mg) (Fig. 1a). This uptake was shown to be specific by blocking with excess DFO-thyrotropin-alfa, significantly reducing ($P < 0.0001$) uptake in THJ529T + cells (1.8 ± 0.4% bound/mg) (Fig. 1a). Uptake in FTC133 + cells (3.5 ± 0.5% bound/mg) was also significantly higher ($P < 0.0001$) than uptake in FTC133- cells (2.0 ± 0.4% bound/mg) (Fig. 1b). A significant reduction ($P < 0.0001$) in FTC133 + uptake (1.6 ± 0.2% bound/mg) by blocking with excess DFO-thyrotropin-alfa confirmed receptor specificity (Fig. 1b).

The binding affinity (K_d) of [^{89}Zr]Zr-thyrotropin-alfa was determined to be 99 nM (95% CI = 90–109 nM) by a radioactive binding assay (Fig. 1c). Internalization was assessed in THJ592T + cells and reported as percent internalized. The percent internalization at 5, 30, 60, and 120 min was 7.5 ± 3.0%, 30.4 ± 10.0%, 40.5 ± 2.6%, 41 ± 7.0%, and 50.2 ± 10.0%, respectively (Fig. 1d).

In Vivo PET Imaging

PET images were acquired for female and male mice (Figs. 2 and 3, Fig. S2-7) on Days 1–3 post-injection of 2 µg (1.6 ± 0.1 MBq) [^{89}Zr]Zr-thyrotropin-alfa. SUV_{mean} was calculated as a semi-quantitative approach to describe tumor uptake and *in vivo* biodistribution and is reported for major organs (Tables S1-3).

Representative PET images in the female FTC133 xenograft model, including axial sections of the tumors (Fig. 2a) and whole body coronal slices (Fig. 3), are shown. Tumor uptake in FTC133 + tumors is distinct from FTC133- tumors (Fig. 2a), as supported by significant differences in SUV_{mean} between FTC133 + and FTC133- tumors (Fig. 2b). SUV_{mean} in FTC133 + tumors on Day 1 (0.31 ± 0.02), Day 2 (0.24 ± 0.01), and Day 3 (0.20 ± 0.01) post-injection were significantly higher ($P < 0.0001$) than uptake in FTC133- tumors on Day 1 (0.09 ± 0.02), Day 2 (0.06 ± 0.01), and Day 3 (0.06 ± 0.01) post-injection. Tumor uptake can also be visualized in whole body PET images (Fig. 3), which showed high uptake in the liver and kidney relative to the tumor. SUV_{mean} for the liver,

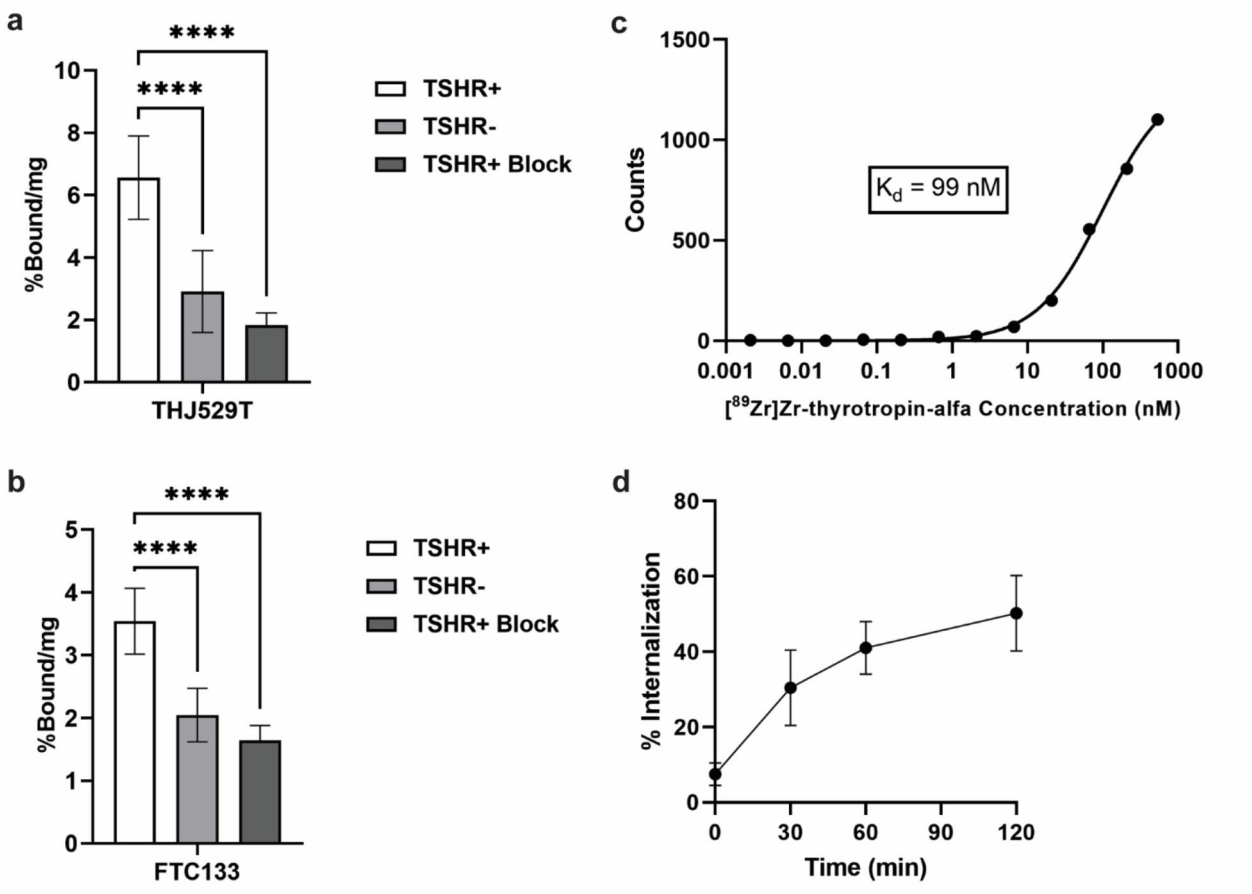

Fig. 1. *In vitro* [^{89}Zr]Zr-thyrotropin-alfa uptake. **a)** Uptake in THJ529T cells with 250 nM DFO-thyrotropin-alfa block ($n=6$). **b**) Uptake in FTC133 cells with 250 nM DFO-thyrotropin-alfa block ($n=6$). **c**) Binding affinity determined by a radioactive binding assay ($n=2$). **d**) Internalization in THJ529T + cells ($n=6$). Data is presented as mean ± standard deviation. ****$P<0.0001$.

kidney, and other major organs for Days 1–3 post-injection are summarized in Tables S1-3. On Day 2 post-injection, kidney uptake in the FTC133- model (5.6 ± 0.4) was significantly higher ($P<0.05$) than uptake in the FTC133 + model (4.5 ± 0.3) (Table S2). On Day 3 post-injection, liver uptake in the FTC133 + model ($P<0.05$) was significantly higher (2.8 ± 0.3) than uptake in the FTC133- model (1.6 ± 0.4) (Table S3). SUV_{mean} in other organs, including bone, heart, and muscle, remained low on Days 1–3 post-injection and did not differ amongst xenograft models.

Whole body PET imaging in the female THJ529T xenograft model (Fig. S5), male FTC133 xenograft model (Fig. S6), and male THJ529T xenograft model (Fig. S7) showed a similar pattern of biodistribution as the female FTC133 xenograft model (Fig. 3), with the highest uptake in the liver and kidneys and low uptake in other major organs, aside from the tumor (Tables S1-3).

PET imaging of tumors in the female THJ529T xenograft model (Fig. S2a) showed significant differences in SUV_{mean} on Days 1–3 post-injection (Fig. S2b). On Day 1 post-injection, uptake in THJ529T + tumors (0.33 ± 0.04) was significantly higher ($P<0.05$) than THJ529T- tumors (0.23 ± 0.02). Uptake in THJ529T + tumors was also significantly higher on Day 2 post-injection ($P<0.05$) and Day 3 post-injection ($P<0.001$) (Fig. S2b). SUV_{mean} in THJ529T + tumors was 0.22 ± 0.03 on Day 2 post-injection and 0.19 ± 0.01 on Day 3 post-injection, compared to 0.15 ± 0.02 on Day 2 post-injection and 0.12 ± 0.01 on Day 3 post-injection in THJ529T- tumors (Fig. S2b).

Similar patterns of uptake for TSHR + and TSHR- tumors were seen in the male FTC133 xenograft model (Fig. S3a) and male THJ529T xenograft model (Fig. S4a). In the male FTC133 xenograft model (Fig. S3), FTC133 + tumor uptake (0.35 ± 0.02) was significantly higher ($P<0.05$) than FTC133- tumor uptake (0.15 ± 0.09) on Day 1 post-injection (Fig. S3b). FTC133 + tumor uptake on Day 2 post-injection (0.29 ± 0.02) and Day 3 post-injection (0.25 ± 0.01) was also significantly higher ($P<0.0001$) than FTC133- tumor uptake on Day 2 (0.08 ± 0.02) or Day 3 post-injection (0.08 ± 0.02) (Fig. S3b). In the male THJ529T xenograft model (Fig. S4), THJ529T + tumor uptake (0.41 ± 0.05) was significantly higher ($P<0.01$) than THJ529T- tumor uptake (0.25 ± 0.03) on Day 1 post-injection (Fig. S4b). THJ529T + tumor uptake on Day 2 post-injection (0.29 ± 0.05) and Day 3 post-injection (0.25 ± 0.04) was also significantly higher ($P<0.05$) than THJ529T- tumor uptake on Day 2 (0.18 ± 0.04) or Day 3 post-injection (0.15 ± 0.02) (Fig. S4b).

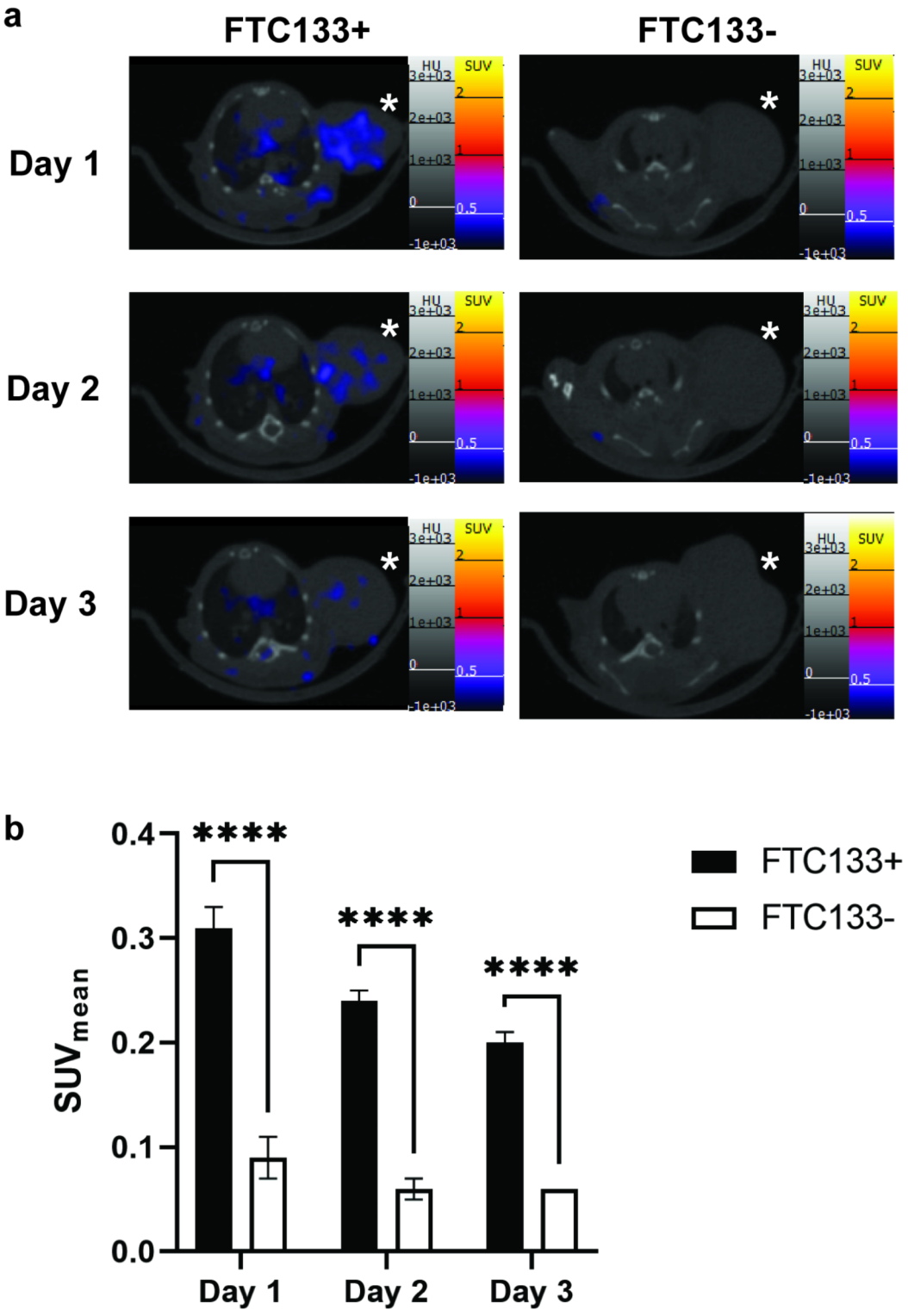

Fig. 2. PET imaging of tumors in female athymic nude mice bearing FTC133 xenografts. **a**) Representative axial sections of female athymic nude mice bearing FTC133 xenografts (*) implanted in the left shoulder on Days 1–3 post-injection. Images were windowed the same for comparison. **b**) SUV_{mean} (mean ± SD) in the FTC133 tumors on Days 1–3 post-injection ($n = 4$). $P < 0.0001$ =****.

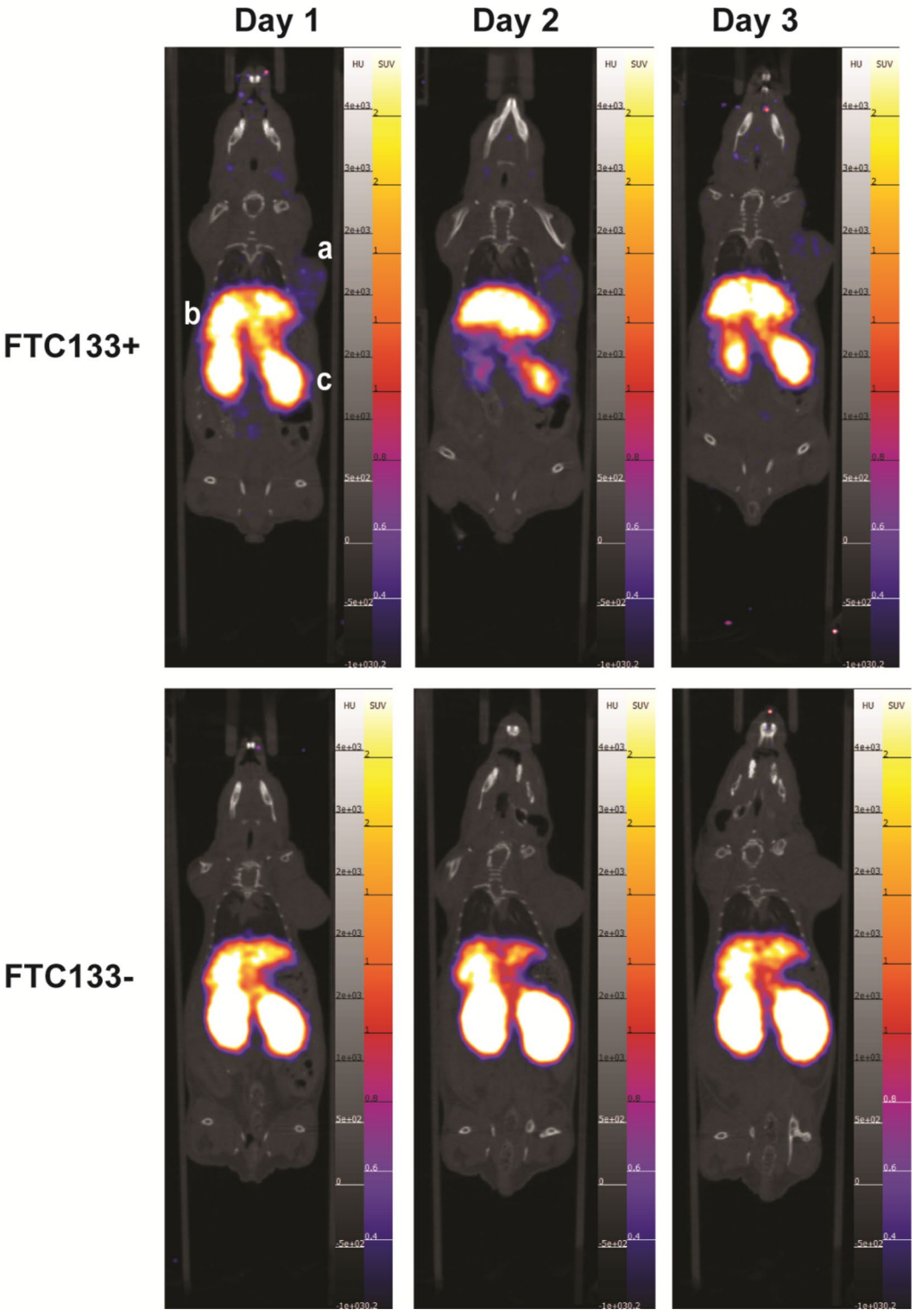

Fig. 3. Whole body PET imaging in female athymic nude mice bearing FTC133 xenografts. Representative coronal sections of female athymic nude mice bearing FTC133 xenografts implanted in the left shoulder on Days 1–3 post-injection. The tumor (**a**), liver (**b**), and kidneys (**c**) are noted. Images were windowed the same for comparison.

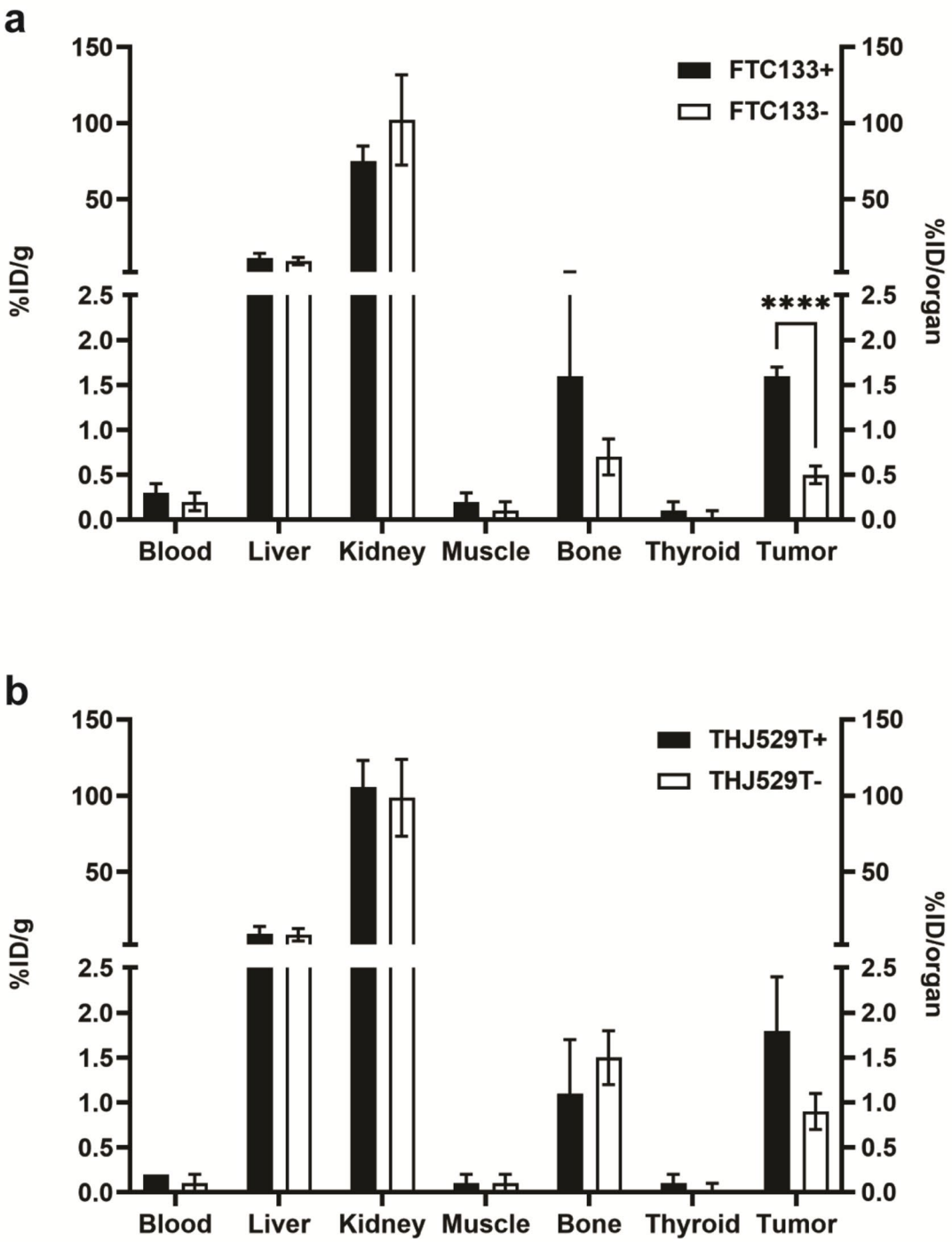

Fig. 4. *Ex vivo* biodistribution on Day 3 post-injection in female athymic nude mice bearing FTC133(**a**)and THJ529T(**b**) xenografts. Data is presented as mean ± STD ($n = 4$) % ID/g of tissue, except thyroid, which is presented as % ID/organ. $P < 0.0001$ =****.

Ex Vivo Biodistribution

After imaging on Day 3 post-injection, mice were euthanized and organs were collected for biodistribution analysis. The complete biodistribution is provided for female (Table S4) and male (Table S5) mice, with major organs highlighted for female (Fig. 4) and male (Fig. S8) mice. The thyroid was grossly resected from the anterior neck with the surrounding tissue and is reported as % ID/organ. All other organs are reported as % ID/g.

In the FTC133 xenograft model, there was a significant difference between FTC133 + and FTC133- tumors in female mice ($P < 0.0001$) (Fig. 4a) and male mice ($P < 0.0001$) (Fig. S8a), consistent with the difference in SUV_{mean} on Day 3 (Fig. 2, Fig. S3). % ID/g in FTC133 + female mice was 1.6 ± 0.1% ID/g compared to 0.5 ± 0.1%

ID/g in FTC133- female mice (Fig. 4a). A similar difference in % ID/g was seen in male mice in FTC133+ (1.3 ± 0.1% ID/g) and FTC133- (0.4 ± 0.1% ID/g) tumors (Fig. S8a).

In the THJ529T xenograft model, there was no significant difference ($P > 0.05$) between THJ529T + and THJ529T- tumors in female mice (Fig. 4B) or male mice (Fig. S8b) as determined by the biodistribution, despite evidence of a trend of higher % ID/g for both female and male mice with THJ529T + tumors. THJ529T + tumors in female mice had 1.8 ± 0.6% ID/g compared to 0.9 ± 0.2% ID/g in THJ529T- tumors (Fig. 4b). For male mice, THJ529T + tumors had 1.2 ± 0.3% ID/g compared to 0.9 ± 0.2% ID/g in THJ529T- tumors (Fig. S8b).

Organs with the highest % ID/g were the liver and kidneys across all xenograft models (Fig. 4, Fig. S8), as supported by whole body PET imaging on Days 1–3 post-injection (Fig. 3, Fig. S5-7). For female mice (Fig. 4), % ID/g in the liver ranged from 9.0 ± 4.1 (THJ529T-) to 12.0 ± 2.9 (FTC133+). In male mice (Fig. S8), % ID/g in the liver was lower on average, ranging from 5.2 ± 2.1% ID/g (THJ529T-) to 7.0 ± 1.0% ID/g (FTC133-). Similar sex differences were seen in the kidney, with a range of 75.0 ± 10.1 (FTC133+) to 106 ± 17.4 (THJ529T+) in female mice and 34.0 ± 5.8 (FTC133+) to 62.0 ± 14.0 (THJ529T-) in male mice. Aside from sex differences in the liver and kidney, there was no significant differences in % ID/g for organs within xenograft models except for kidney uptake in male mice bearing FTC133 tumors ($P < 0.05$).

Discussion

This study represents a preclinical evaluation of thyroid-stimulating hormone receptor (TSHR)-targeted [^{89}Zr]Zr-thyrotropin-alfa, in which uptake of [^{89}Zr]Zr-thyrotropin-alfa was assessed through a combination of *in vitro* cell uptake, *in vivo* PET imaging, and *ex vivo* biodistribution. TSHR-targeted radiopharmaceuticals, such as [^{89}Zr]Zr-thyrotropin-alfa, have the potential to offer an important theranostic alternative for patients with radioiodine refractory disease, in particular due to the FDA-approval and routine clinical use of thyrotropin-alfa, a recombinant human TSH analogue[17,18].

In this study, i*n vitro* cell uptake of [^{89}Zr]Zr-thyrotropin-alfa demonstrated rapid internalization with preferential and specific uptake in cell lines expressing the TSHR. *In vivo* PET imaging and *ex vivo* biodistribution in male and female mice bearing THJ529T or FTC133 xenografts showed significant uptake in TSHR + xenografts, which was highest on Day 1 post-injection. Low uptake in the lungs on Day 1 post-injection, a common site of DTC metastasis[30], also allowed for clear visualization of the thoracic cavity. Clearance from the TSHR + xenografts on Day 2 and Day 3 post-injection limits the benefit of imaging beyond Day 1 post-injection. Aside from the tumor, organs with the highest uptake of [^{89}Zr]Zr-thyrotropin-alfa were the liver and kidney, a likely route of metabolism and excretion consistent with other protein-based radiopharmaceuticals and recombinant human TSH analogues[12,13,31,32]. With regard to sex, no significant differences were seen in tumor uptake between male and female mice. There was, however, 50% higher % ID/g in the liver and 2-fold higher % ID/g in the kidney in female mice compared to male mice with biodistribution on Day 3 post-injection, likely due to sex-based differences in metabolism and excretion[33].

Importantly, preclinical SPECT imaging in a mouse model with radioiodinated thyrotropin-alfa has been previously reported[19]. Using ^{123}I ($t_{1/2}$ = 13.2 h), mice were injected with 10 µg [^{123}I]I-thyrotropin-alfa and imaged up to three hours post-injection[19]. At one hour post-injection, authors reported an average % ID/g of 14.1 ± 1.6 in the blood, 3.6 ± 0.4 in the heart, 5.3 ± 0.7 in the liver, and 34.0 ± 7.0 in the kidney. With [^{89}Zr]Zr-thyrotropin-alfa, the % ID/g on Day 3 post-injection was similar to [^{123}I]I-thyrotropin-alfa in the liver and kidney, with 6.3 ± 1.2% ID/g and 45.2 ± 4.5% ID/g, respectively. By contrast, uptake in the blood and heart with [^{89}Zr]Zr-thyrotropin-alfa was 70-fold and 5-fold lower at Day 3 post-injection, respectively, suggesting the importance of longer imaging time-points to allow for circulation and non-specific clearance of this tracer. Aside from the biodistribution, the potential for comparison in tumor uptake between radioiodinated thyrotropin-alfa and [^{89}Zr]Zr-thyrotropin-alfa is more limited due to differences in study design, most notably the selection of cell line, imaging time-points, and injected mass dose[19].

In addition to thyrotropin-alfa, preclinical PET imaging with recombinant human TSH analogue TR1402 has been previously reported[12,13]. TR1402 is a larger (28 kDa) recombinant human thyroid-stimulating hormone (TSH) analogue, with increased agonism and higher affinity for the TSHR[11,34–36]. Compared to [^{89}Zr]Zr-TR1402, *in vivo* uptake with [^{89}Zr]Zr-thyrotropin-alfa was only moderately lower in the tumor, suggesting comparable potential in TSHR + tumor targeting. This moderate difference is illustrated on Day 1 post-injection with an average SUV_{mean} of 0.44 ± 0.06 in TSHR + male mice and 0.37 ± 0.05 in TSHR + female mice with [^{89}Zr]Zr-TR1402 and an average SUV_{mean} of 0.38 ± 0.04 in TSHR + male mice and 0.34 ± 0.03 in TSHR + female mice with [^{89}Zr]Zr-thyrotropin-alfa. However, % ID/g in the kidney was 2-fold higher in female mice with [^{89}Zr]Zr-thyrotropin-alfa compared to [^{89}Zr]Zr-TR1402, despite comparable biodistribution in the liver.

A limitation of this study was the use of stably transduced cell lines, which may not reflect the level of TSHR expression in all patients. However, results from SPECT imaging with radioiodinated thyrotropin-alfa[19] suggest future studies with endogenously expressing patient xenografts would be worthwhile for further preclinical validation.

In conclusion, this study represents a preclinical evaluation of thyroid-stimulating hormone receptor (TSHR)-targeted PET radiopharmaceutical [^{89}Zr]Zr-thyrotropin-alfa using an FDA approved pharmaceutical. Moderately lower tumor uptake, higher kidney uptake, and the lower affinity of [^{89}Zr]Zr-thyrotropin-alfa may limit future application relative to other protein-based TSHR-targeted radiopharmaceuticals, such as [^{89}Zr]Zr-TR1402, however, the use of an FDA approved agent may allow for a faster path forward for imaging clinical trials with this tracer on Day 1 post-injection.

Data availability

All data generated or analyzed during the study are included in the published paper.

Received: 6 September 2024; Accepted: 18 March 2025
Published online: 03 April 2025

References

1. Siegel, R. L., Miller, K. D., Wagle, N. S. & Jemal, A. Cancer statistics, 2023. *Cancer J. Clin.* **73**, 17–48. https://doi.org/10.3322/caac.21763 (2023).
2. Baloch, Z. W. et al. Overview of the 2022 WHO classification of thyroid neoplasms. *Endocr. Pathol.* **33**, 27–63. https://doi.org/10.1007/s12022-022-09707-3 (2022).
3. Kitahara, C. M. & Schneider, A. B. Epidemiology of thyroid cancer. *Cancer epidemiology, biomarkers & prevention: a publication of the American association for cancer.Research. Cosponsored Am. Soc. Prev. Oncol.* **31**, 1284–1297. https://doi.org/10.1158/1055-9965.epi-21-1440 (2022).
4. Haugen, B. R. et al. American Thyroid Association Management Guidelines for Adult Patients with Thyroid Nodules and Differentiated Thyroid Cancer: The American Thyroid Association Guidelines Task Force on Thyroid Nodules and Differentiated Thyroid Cancer. *Thyroid: official journal of the American Thyroid Association* 26, 1-133, (2015). https://doi.org/10.1089/thy.2015.0020 (2016).
5. Avram, A. M., Zukotynski, K., Nadel, H. R. & Giovanella, L. Management of differentiated thyroid cancer: the standard of care. *J. Nuclear Medicine: Official Publication Soc. Nuclear Med.* **63**, 189–195. https://doi.org/10.2967/jnumed.121.262402 (2022).
6. Tuttle, R. M. et al. Controversies, consensus, and collaboration in the use of (131)I therapy in differentiated thyroid cancer: A joint statement from the American thyroid association, the European association of nuclear medicine, the society of nuclear medicine and molecular imaging, and the European thyroid association. *Thyroid: Official J. Am. Thyroid Association*. **29**, 461–470. https://doi.org/10.1089/thy.2018.0597 (2019).
7. Durante, C. et al. Long-term outcome of 444 patients with distant metastases from papillary and follicular thyroid carcinoma: benefits and limits of radioiodine therapy. *J. Clin. Endocrinol. Metab.* **91**, 2892–2899. https://doi.org/10.1210/jc.2005-2838 (2006).
8. Worden, F. Treatment strategies for radioactive iodine-refractory differentiated thyroid cancer. *Therapeutic Adv. Med. Oncol.* **6**, 267–279. https://doi.org/10.1177/1758834014548188 (2014).
9. Nixon, I. J. et al. The impact of distant metastases at presentation on prognosis in patients with differentiated carcinoma of the thyroid gland. *Thyroid: Official J. Am. Thyroid Association*. **22**, 884–889. https://doi.org/10.1089/thy.2011.0535 (2012).
10. Kleinau, G. et al. Structural-Functional features of the Thyrotropin receptor: A class A G-Protein-Coupled receptor at work. *Front. Endocrinol.* **8**, 86. https://doi.org/10.3389/fendo.2017.00086 (2017).
11. Galli, F. et al. In vivo imaging of thyroid cancer with (99m)Tc-TR1401 and (99m)Tc-TR1402: A comparison study in dogs. *J. Clin. Med.* **10** https://doi.org/10.3390/jcm10091878 (2021).
12. Gimblet, G. R. et al. Thyroid-stimulating hormone receptor (TSHR) as a target for imaging differentiated thyroid cancer. *Surgery* **175**, 199–206. https://doi.org/10.1016/j.surg.2023.05.045 (2024).
13. Gimblet, G. R. et al. PET imaging of differentiated thyroid cancer with TSHR-Targeted [(89)Zr]Zr-TR1402. *Mol. Pharm.* https://doi.org/10.1021/acs.molpharmaceut.4c00224 (2024).
14. Zhang, Y. et al. Targeting Thyroid-Stimulating hormone receptor: A perspective on Small-Molecule modulators and their therapeutic potential. *J. Med. Chem.* **67**, 16018–16034. https://doi.org/10.1021/acs.jmedchem.4c01525 (2024).
15. Li, H. et al. CAR-T cells targeting TSHR demonstrate safety and potent preclinical activity against differentiated thyroid cancer. *J. Clin. Endocrinol. Metab.* **107**, 1110–1126. https://doi.org/10.1210/clinem/dgab819 (2022).
16. Haugen, B. R. et al. A comparison of Recombinant human Thyrotropin and thyroid hormone withdrawal for the detection of thyroid remnant or cancer. *J. Clin. Endocrinol. Metab.* **84**, 3877–3885. https://doi.org/10.1210/jcem.84.11.6094 (1999).
17. Haugen, B. R. et al. Expanding indications for Recombinant human TSH in thyroid cancer. *Thyroid: Official J. Am. Thyroid Association*. **18**, 687–694. https://doi.org/10.1089/thy.2008.0162 (2008).
18. Coerts, H. I., de Keizer, B., Marlowe, R. J. & Verburg, F. A. Recombinant or endogenous thyroid-stimulating hormone for radioactive iodine therapy in thyroid cancer: state of knowledge and current controversies. *Eur. J. Endocrinol.* **188** https://doi.org/10.1093/ejendo/lvad006 (2023).
19. Corsetti, F. et al. Radioiodinated Recombinant human TSH: a novel radiopharmaceutical for thyroid cancer metastases detection. *Cancer Biother. Radiopharm.* **19**, 57–63. https://doi.org/10.1089/108497804773391685 (2004).
20. Rahmim, A. & Zaidi, H. PET versus SPECT: strengths, limitations and challenges. *Nucl. Med. Commun.* **29**, 193–207. https://doi.org/10.1097/MNM.0b013e3282f3a515 (2008).
21. Queern, S. L. et al. Production of Zr-89 using sputtered yttrium coin targets (89)Zr using sputtered yttrium coin targets. *Nucl. Med. Biol.* **50**, 11–16. https://doi.org/10.1016/j.nucmedbio.2017.03.004 (2017).
22. Chang, A. J. et al. 89Zr-Radiolabeled trastuzumab imaging in orthotopic and metastatic breast tumors. *Pharmaceuticals (Basel Switzerland)*. **5**, 79–93. https://doi.org/10.3390/ph5010079 (2012).
23. Meireles, A. M. et al. Molecular and genotypic characterization of human thyroid follicular cell carcinoma-derived cell lines. *Thyroid: Official J. Am. Thyroid Association*. **17**, 707–715. https://doi.org/10.1089/thy.2007.0097 (2007).
24. Pilli, T., Prasad, K. V., Jayarama, S., Pacini, F. & Prabhakar, B. S. Potential utility and limitations of thyroid cancer cell lines as models for studying thyroid cancer. *Thyroid: Official J. Am. Thyroid Association*. **19**, 1333–1342. https://doi.org/10.1089/thy.2009.0195 (2009).
25. van Staveren, W. C. et al. Human thyroid tumor cell lines derived from different tumor types present a common dedifferentiated phenotype. *Cancer Res.* **67**, 8113–8120. https://doi.org/10.1158/0008-5472.can-06-4026 (2007).
26. Williams, D. W. & Wynford-Thomas, D. Human thyroid epithelial cells. *Methods Mol. Biology (Clifton N J)*. **75**, 163–172. https://doi.org/10.1385/0-89603-441-0:163 (1997).
27. Marlow, L. A. et al. Methodology, criteria, and characterization of Patient-Matched thyroid cell lines and Patient-Derived tumor xenografts. *J. Clin. Endocrinol. Metab.* **103**, 3169–3182. https://doi.org/10.1210/jc.2017-01845 (2018).
28. Goretzki, P. E., Frilling, A., Simon, D. & Roeher, H. D. Growth regulation of normal thyroids and thyroid tumors in man. *Recent. Results cancer Res. Fortschr. Der Krebsforschung Progres Dans Les Recherches Sur Le cancer*. **118**, 48–63. https://doi.org/10.1007/978-3-642-83816-3_6 (1990).
29. Gimblet, G. R. et al. *PET Imaging of Differentiated Thyroid Cancer with TSHR-Targeted [^{89}Zr]Zr-TR1402* (Molecular pharmaceutics Accepted for Publication, 2024).
30. Song, H. J., Xue, Y. L., Xu, Y. H., Qiu, Z. L. & Luo, Q. Y. Rare metastases of differentiated thyroid carcinoma: pictorial review. *Endocr. Relat. Cancer*. **18**, R165–174. https://doi.org/10.1530/erc-11-0068 (2011).
31. Ducharme, M. et al. Evaluation of [(89)Zr]Zr-DFO-2Rs15d nanobody for imaging of HER2-Positive breast cancer. *Mol. Pharm.* **20**, 4629–4639. https://doi.org/10.1021/acs.molpharmaceut.3c00360 (2023).
32. Kasten, B. B. et al. Positron emission tomography imaging with (89)Zr-labeled anti-CD8 cys-diabody reveals CD8(+) cell infiltration during oncolytic virus therapy in a glioma murine model. *Sci. Rep.* **11**, 15384. https://doi.org/10.1038/s41598-021-94887-x (2021).
33. Czerniak, R. Gender-based differences in pharmacokinetics in laboratory animal models. *Int. J. Toxicol.* **20**, 161–163. https://doi.org/10.1080/109158101317097746 (2001).

34. Leitolf, H., Tong, K. P., Grossmann, M., Weintraub, B. D. & Szkudlinski, M. W. Bioengineering of human Thyrotropin superactive analogs by site-directed lysine-scanning mutagenesis. Cooperative effects between peripheral loops. *J. Biol. Chem.* **275**, 27457–27465. https://doi.org/10.1074/jbc.M003707200 (2000).
35. Reinfelder, J. et al. Effects of Recombinant human thyroid-stimulating hormone superagonists on thyroidal uptake of 18F-fluorodeoxyglucose and Radioiodide. *Thyroid: Official J. Am. Thyroid Association*. **21**, 783–792. https://doi.org/10.1089/thy.2010.0394 (2011).
36. Faust, B. et al. Autoantibody mimicry of hormone action at the Thyrotropin receptor. *Nature* **609**, 846–853. https://doi.org/10.1038/s41586-022-05159-1 (2022).

Acknowledgements

The authors would like to thank the UAB cyclotron facility for production of zirconium-89. UAB is a member of the DOE University Isotope Network and is supported by DESC0021269. P.R. was partially supported by the Education and Research Foundation for Nuclear Medicine and Molecular Imaging through SNMMI and the UAB Summer Research Academy. Funding for this project and PET imaging studies were supported by The O'Neal Comprehensive Cancer Center at UAB through P30 CA013148.

Author contributions

G.R.G. performed the experiments with assistance from P.R., M.M.H., H.A.H., J.W., J.A.C., and S.S.K. G.R.G. analyzed the data and wrote the manuscript. R.JS., and S.E.L. supervised the project. All authors reviewed the manuscript.

Funding

This original research manuscript was supported though O'Neal Invests Pre-R01 and the National Cancer Institute (NCI) Cancer Center Support Grant P30 CA013148, which enabled PET/CT imaging through UAB's Preclinical Imaging Shared Facility. P.R. was partially supported by the Education and Research Foundation for Nuclear Medicine and Molecular Imaging through SNMMI and the UAB Summer Research Academy.

Declarations

Competing interests

The authors declare no competing interests.

Additional information

Supplementary Information The online version contains supplementary material available at https://doi.org/10.1038/s41598-025-94923-0.

Correspondence and requests for materials should be addressed to R.J.-S. or S.E.L.